JOURNAL OF THE AMERICAN CHEMICAL SOCIETY

Communication

pubs.acs.org/JACS

Oxygen-Assisted Chemical Vapor Deposition Growth of Large Single-Crystal and High-Quality Monolayer MoS_2

Wei Chen,[†,‡,∥] Jing Zhao,[†,∥] Jing Zhang,[†,∥] Lin Gu,[†,§] Zhenzhong Yang,[†] Xiaomin Li,[†] Hua Yu,[†] Xuetao Zhu,[†] Rong Yang,[†] Dongxia Shi,[†] Xuechun Lin,[⊥] Jiandong Guo,[†] Xuedong Bai,[†] and Guangyu Zhang*[,†,§]

[†]Beijing National Laboratory for Condensed Matter Physics and Institute of Physics, Chinese Academy of Sciences, Beijing 100190, China

[‡]College of Physics and Electronic Information, Gannan Normal University, Ganzhou, Jiangxi 341000, China

[§]Collaborative Innovation Center of Quantum Matter, Beijing 100190, China

[⊥]Institute of Semiconductors, Chinese Academy of Sciences, Beijing 100083, China

Supporting Information

ABSTRACT: Monolayer molybdenum disulfide (MoS_2) has attracted great interest due to its potential applications in electronics and optoelectronics. Ideally, single-crystal growth over a large area is necessary to preserve its intrinsic figure of merit but is very challenging to achieve. Here, we report an oxygen-assisted chemical vapor deposition method for growth of single-crystal monolayer MoS_2. We found that the growth of MoS_2 domains can be greatly improved by introducing a small amount of oxygen into the growth environment. Triangular monolayer MoS_2 domains can be achieved with sizes up to ~350 μm and a room-temperature mobility up to ~90 $cm^2/(V{\cdot}s)$ on SiO_2. The role of oxygen is not only to effectively prevent the poisoning of precursors but also to eliminate defects during the growth. Our work provides an advanced method for high-quality single-crystal monolayer MoS_2 growth.

Two-dimensional (2D) crystals of transition metal dichalcogenides (TMDs) are an emerging class of materials with unique properties, making them useful as building blocks for novel electronic and optoelectronic devices.[1] For example, monolayer molybdenum disulfide (MoS_2), a representative TMD, has been demonstrated to be very promising for field effect transistors (FETs),[2] spin and valley devices,[3] photodetectors,[4] memristors,[5] and piezotronics.[6] Recently, to obtain an electronic-level monolayer MoS_2, various approaches have been developed, including exfoliation from the bulk material,[7] chemical vapor deposition (CVD),[8] and metal−organic CVD.[9] In particular, the CVD approach has potential in low-cost and scaled-up production; thus it has attracted much research interest. However, regardless of different CVD precursors and growth recipes, the MoS_2 monolayer is composed of non-uniform separated triangular domains, with the largest single triangular domain of ~123 μm.[8b] Although polycrystalline films can be obtained on either SiO_2 or sapphire substrates, the crystalline grains are typically <1 μm, and the carrier mobility is rather low due to the presence of a large amount of domain boundaries.[8c,d] Therefore, the growth of large MoS_2 single crystals is highly desired.

Here, we report the successful growth of large-grain and high-quality monolayer MoS_2 on c-face sapphire via an oxygen-assisted (OA) CVD method. The presence of a small amount of oxygen during growth can largely suppress the MoS_2 nucleation density and meanwhile prevent poisoning of the MoO_3 precursor[10] to enable large domain growth. The resulting single-crystal monolayer triangle MoS_2 domains have the largest size of ~350 μm and a room-temperature (RT) mobility of ~90 $cm^2/(V{\cdot}s)$ on SiO_2; both characteristics are the highest ever reported.

The growth of MoS_2 was carried out in a modified CVD setup as depicted in Figure S1. Unlike the widely used setup in which substrates are put face-down above the MoO_3 source, the present setup uses a three-zone furnace for the growth (see experimental details in the Supporting Information). Prior to the growth process, sapphire substrates (c-face) were first rinsed in acetone and isopropanol and then annealed in a vacuum at 1100−1200 °C for 3 h to clean the surface. After annealing, a clean and atomically flat surface is obtained (refer to Figure S2). The surface structure of c-face sapphire has the same symmetry as the MoS_2 lattice structure, thus facilitating the epitaxial growth of single-crystal MoS_2. 100-sccm Ar and a small amount of O_2 were used as carrier gas, and the growth pressure was kept at 0.5 Torr. Typical temperatures of sulfur, MoO_3, and the substrate are kept at 115, 530, and 850 °C, respectively, during growth. Figure 1a−c shows optical microscopy images of MoS_2 grown on sapphire substrates for 30 min with the O_2 flow rate varying from 0 to 2 sccm. From the atomic force microscopy (AFM) image in Figure 1a, we can clearly see that a large amount of MoS_2 particles were grown on both the substrate and MoS_2 when no oxygen carrier gas was introduced. As a comparison, a uniform and 100% coverage monolayer MoS_2 film was achieved with 1-sccm O_2 introduced into the growth chamber (Figure 1b). The zoomed-in AFM image of Figure 1b shows that the substrate is fully covered, clean (contamination-free), uniform (wrinkle-free), and ultraflat, with a surface roughness ~0.1 nm. Those terraces showing in the

Received: October 8, 2015
Published: December 1, 2015

ACS Publications © 2015 American Chemical Society

DOI: 10.1021/jacs.5b10519
J. Am. Chem. Soc. 2015, 137, 15632−15635

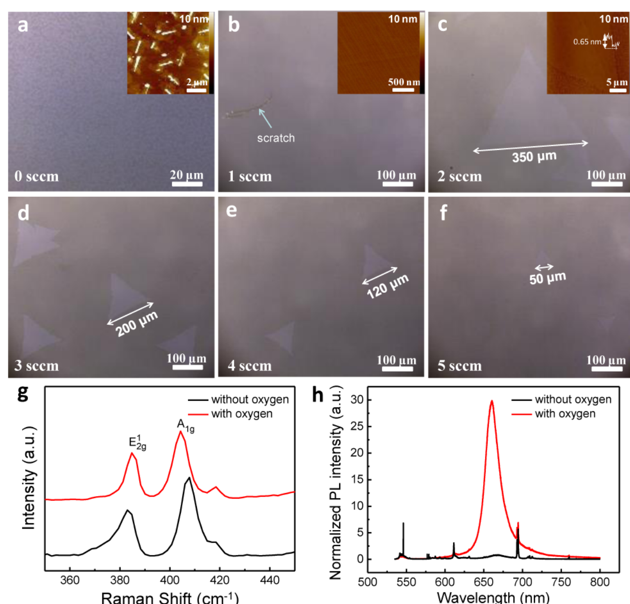

Figure 1. Growth of monolayer MoS_2 films and large domains at variable oxygen flow rates. (a−f) Optical images of MoS_2 grown on sapphire for 30 min with O_2 flow rate ranging from 0 to 5 sccm. The side length of the triangular domain is ∼350 μm in panel c. The insets in (a−c) are AFM height images of MoS_2 grown on sapphire under different O_2 flow rates (0−2 sccm). A height profile was extracted along the dashed line shown in panel c. The single domain thickness is ∼0.65 nm, equal to a monolayer thickness. (g,h) Typical Raman (g) and photoluminescence (h) spectra of as-grown MoS_2 with (red) and without (black) O_2 carrier gas, respectively.

image reflect the stepped surface of c-face sapphire, as shown in Figure S3. These results suggest that the small amount of oxygen could etch off unsteady nuclei and suppress the growth of nanoparticles or nanotubes.[11] The chemical composition of the monolayer MoS_2 film was confirmed by X-ray photoelectron spectroscopy (XPS; see Figure S5).

With further increasing the O_2 flow rate to 2 sccm, the side length of triangular domain can be as large as ∼350 μm, with a lateral growth rate of ∼12 μm/min (Figure 1c). To our knowledge, ∼350 μm is the largest lateral size of 2D MoS_2 single crystals ever achieved. The clean surface of these MoS_2 domains reveals that the adsorption of vaporized precursors on the MoS_2 basal plane is not allowed for additional layer growth under this growth condition. The MoS_2 edges are only reactive to facilitate the enlargement of MoS_2 domains. Note that those small and dense MoS_2 nuclei are formed during the cooling-down stage of the growth process. It is also found that the nucleation density and the maximum domain size of as-grown MoS_2 drop gradually when the O_2 flow rate is further increased from 3 to 5 sccm (Figure 1d−f).

Raman and photoluminescence (PL) spectra of as-grown MoS_2 samples are shown in Figure 1g,h. The characteristic Raman peaks of MoS_2 grown with O_2 locate at 384.6 cm^{-1} (in-plane E_{2g} mode) and 404.3 cm^{-1} (out-of-plane A_{1g} mode). As a comparison, they are at 383.0 and 407.8 cm^{-1} for samples grown without O_2. This narrower frequency difference between the two Raman peaks (Δ) in the former case is ∼20 cm^{-1}, suggesting the monolayer nature.[12] The PL spectra of the MoS_2 samples grown with O_2 show a single sharp excitonic A peak at ∼660 nm (1.88 eV). The strong PL intensity and narrow full width at half-maximum indicate insignificant defect formation and the monolayer nature of MoS_2.[8b,13]

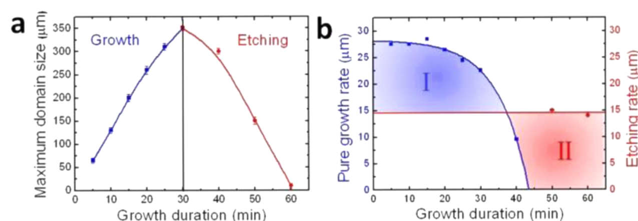

Figure 2. Effect of oxygen on the domain size at various growth durations. (a) Evolution of the size of single-crystal MoS_2 domains as a function of the growth duration. The blue and red lines represent the fitting curves. The error bars indicate the variation in size. Typical MoS_2 domains grown on sapphire under 2-sccm O_2 with various growth durations are presented in Figure S8. (b) Dependence of pure growth rate and etching rate of MoS_2 domains on the growth duration. Domain size = growth duration × (growth rate − etching rate). The blue I and red II regions represent dominant growth and etching during the growth process, respectively.

To see the effect of oxygen during the growth, we investigated the MoS_2 growth under 2-sccm O_2 flow rate with various growth durations (Figure S8). The average side lengths (l) of the MoS_2 domains are plotted as a function of growth duration (Figure 2a). We can see that the nucleation density of MoS_2 grains is very low at the beginning (Figure S8a). With increasing growth duration, l increases (Figure S8b−f). Typically $l \approx 125$, 275, and 350 μm after growth for 10, 20, and 30 min, respectively. Notably, a further increase of growth duration would lead to etching of the as-grown domains, as seen by the gradually decreasing domain sizes (Figure S8g−i) and the etched triangular pits as well (Figure S9). In particular, the as-grown MoS_2 domains can be almost completely etched off after 60 min growth. Besides, the aligned triangular pits in a single domain also indicate the single-crystal nature of these domains.

During growth, MoO_3 is reduced by sulfur to facilitate MoS_2 deposition on substrate surface.[8f] It has been demonstrated that the anisotropic oxidative etching of MoS_2 is closely related to temperature, and oxidation at 400 °C results in complete conversion to MoO_3.[14] In our growth process, a small amount of O_2 is mixed in Ar as carrier gas, and the nucleation density of MoS_2 is substantially decreased through etching off of unsteady nucleus and chemical oxidation of its edges, where the Mo and S atoms become MoO_3 and SO_2 gas molecules. Thus, the growth process is accompanied by the O_2 etching effect.

The relationship between the rates of pure growth/etching of MoS_2 domains and growth duration is demonstrated in Figure 2b. The blue line shows that the growth rate is nearly constant in the early growth process (<15 min), and then it gradually decreases. The etching rate is assumed to be constant, depending only on the oxygen flow rate. As a result, the growth of MoS_2 is only allowed when the growth rate is higher than the etching rate (blue I region). Notably, on further increase of the growth duration (>30 min), the etching dominates, and the MoS_2 domains start to shrink dramatically (red II region).

In spite of the etching effect, oxygen helps by preventing the sulfurization of the MoO_3 source and guarantees its continuous evaporation during growth. As we all know, MoS_2 has a higher melting point than MoO_3; once the MoO_3 source is sulfured, evaporation stops at the temperature mentioned above. This is a typical source poisoning process which should be avoided.[10] During our growth process, the MoO_3 source is protected by oxygen and can evaporate continuously to prevent poisoning. The long lifetime of the MoO_3 source enables us to effectively grow MoS_2 with very large domain sizes.

DOI: 10.1021/jacs.5b10519
J. Am. Chem. Soc. 2015, 137, 15632−15635

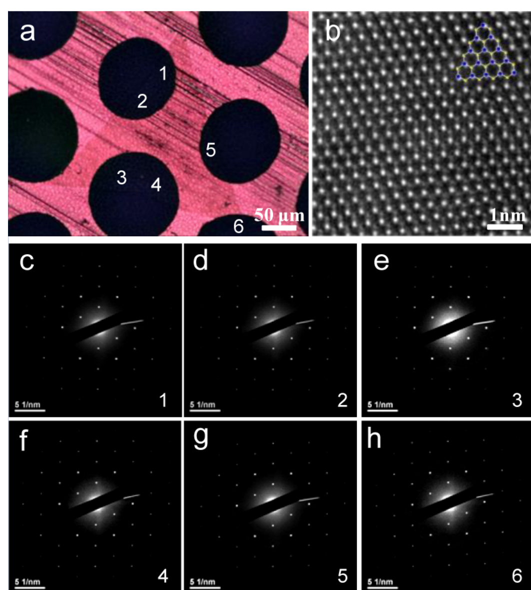

Figure 3. Structural characterizations of single MoS_2 domains. (a) Optical image of the MoS_2 domain transferred onto a TEM grid. (b) Atomic resolution ADF-STEM image of monolayer MoS_2, with the structural model overlaid. The bright and gray spots indicate molybdenum and two stacked sulfur atoms, respectively. (c−h) SAED patterns acquired from different areas on the TEM grid labeled 1−6. These SAED data confirm the single-crystalline nature of the MoS_2, as they show the same set of six-fold-symmetric diffraction points.

To clarify the structure of monolayer MoS_2 domains on sapphire, we carried out transmission electron microscopy (TEM) characterizations. An optical image of a single-domain MoS_2 sample transferred onto a TEM grid is shown in Figure 3a. With aberration-corrected annular dark-field scanning transmission electron microscopy (ADF-STEM), we are able to image the atomic structure of single-crystal MoS_2 domains, as shown in Figure 3b. The brighter/dimmer areas correspond to Mo/S atoms. From these high-resolution images, we can see that the single-crystal MoS_2 domain has a nearly perfect lattice structure and that vacancies, topological defects, and dislocations are rarely seen. The selected area electron diffraction (SAED) patterns acquired from six representative areas in TEM grid windows overlaid by the single domains marked by 1−6 are shown in Figure 3c−h. Hexagonal diffraction spots confirm the presence of MoS_2, and all of the spots have the same crystallographic orientations, displaying a single-crystalline lattice structure of the MoS_2. We looked at many other domains and found similar results. The high crystal quality of MoS_2 domains is attributed to the synergistic effect of the growth and etching.[15]

To evaluate the electrical properties of our single-crystal MoS_2 domains, we transferred these large MoS_2 domains from sapphire onto 300 nm thick SiO_2 substrates by wet chemical etching (see Supporting Information). The typical optical microscopy and AFM images show that the surface of as-transferred single-domain MoS_2 on SiO_2 is very clean and flat (Figures 4a,b and S12). The AFM image shows that there are only a few particles and wrinkles on the flat surface. FET devices (schematic shown in Figure 4c) were then fabricated and annealed at 450 °C for 4 h in an argon and hydrogen mixture for photoresist residual removal and better contact before electrical measurements in a vacuum. Figure 4d,e shows the output and transfer characteristics of a typical device. The device shows typical n-type behavior, and linear $I-V$ curves demonstrate ohmic-like contact under low

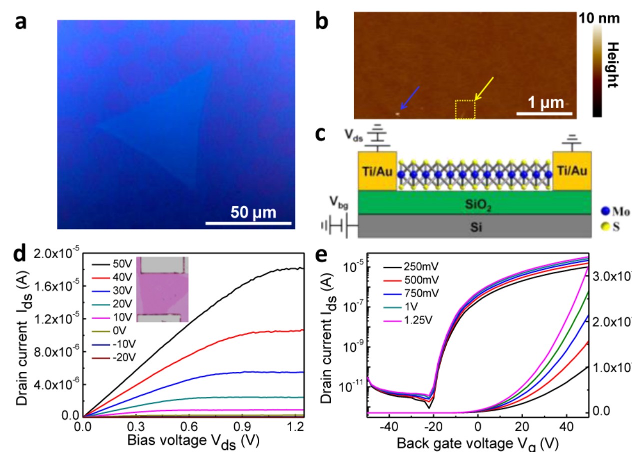

Figure 4. Transferred monolayer MoS_2 single-domain FET devices. (a,b) Optical image and AFM image of a triangle MoS_2 single domain transferred onto SiO_2/Si substrate. (c) Schematic of the monolayer MoS_2 FET device structure. (d) Output characteristics of the device with gate voltages sweeping from −20 to 50 V. Inset: optical image of the device. Device channel length is ~20 μm. (e) Transfer characteristics of the device with gate voltages sweeping from −50 to 50 V and bias varying from 0.25 to 1.25 V. The on/off ratio is ~10^7, and $V_{th} \approx -20$ V.

Table 1. Comparison of Various MoS_2 FETs Fabricated on Si/SiO_2 Substrates[a]

Materials	Growth method	Morphology	Grain size (μm)	Mobility ($cm^2V^{-1}s^{-1}$)	ON/OFF ratio	Reference
MoS_2	Thermal decomposition of $(NH_4)_2MoS_4$	Few layer	<0.1	6	10^5	8h
MoS_2	Pre-deposited Mo film-CVD	Few layer	0.01-0.03	0.004-0.04		8i
MoS_2	Pre-deposited MoO_3 film-CVD	Few layer		0.8	10^5	8j
MoS_2	$MoCl_5$-LPCVD	Monolayer	0.01-0.1	0.003-0.03		8d
MoS_2	Metal-organic CVD	Monolayer	2-3	30	10^6	9
MoS_2	MoO_3-APCVD	Monolayer	123	1-8	10^5-10^7	8b
MoS_2	MoO_3-APCVD	Monolayer	30	45	10^6	2
MoS_2	O_2+MoO_3-LPCVD	Monolayer	350	90	10^7	*This work*

[a]LPCVD, low-pressure chemical vapor deposition; MOCVD, metal−organic chemical vapor deposition; APCVD, atmospheric-pressure chemical vapor deposition.

bias.[16] The maximum I_{on}/I_{off} ratio is >10^7 at RT, and the threshold voltage is around −20 V. In this study, the single-domain MoS_2 FET is configured in a global back-gated geometry. The electron mobility of the device is calculated according to the standard FET model used previously (see Supporting Information).[17] The obtained electron mobility of OACVD-created single-crystal MoS_2 device can be as high as ~90 $cm^2/(V \cdot s)$, which is about double the mobility (45 $cm^2/(V \cdot s)$) reported for an exfoliated or CVD grown MoS_2 domain.[2] It is reported that the sulfur vacancies could trap electrons, acting as charged scattering centers and reducing the electron mobility.[18] In our samples, the high mobility indicates very low sulfur vacancies, in agreement with the TEM characterizations. These results suggest that our MoS_2 has much better crystal quality than previous exfoliated[2] or CVD MoS_2 (Table 1).

We also investigated the growth of MoS_2 on amorphous substrate, e.g., 300 nm SiO_2 on Si, to demonstrate the effectiveness of the OACVD growth method. The optical images and corresponding AFM images of MoS_2 grown under different O_2 flow rates are shown in Figure 5. Without the assistance of O_2, a polycrystalline monolayer of MoS_2 with homogeneous domain size of ~500 nm can be achieved. The growth follows typical 2D

DOI: 10.1021/jacs.5b10519
J. Am. Chem. Soc. 2015, 137, 15632−15635

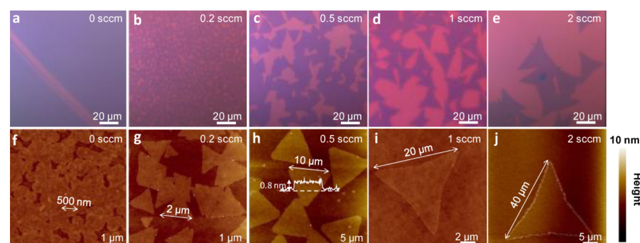

Figure 5. Domain size and shape evolution of MoS_2 on SiO_2 tuned by oxygen carrier gas. (a−e) Optical images of MoS_2 grown on SiO_2 for 10 min under distinct oxygen flow rates of 0, 0.2, 0.5, 1, and 2 sccm, respectively. (f−j) Corresponding AFM images. A height profile was extracted along the dashed line shown in panel h. The single domain thickness is ∼0.8 nm, equal to a monolayer thickness. The shape transfers from roundness in panel f, with size 500 nm in diameter, to triangles in panels g−j, with side lengths ∼2−40 μm.

growth, i.e., nucleation, growth, and coalescence, as reported in our previous work.[8c] However, after introduction of 0.2-sccm O_2, regular triangular domains appear with a side length of ∼2 μm. The nucleation density of MoS_2 decreases with further increasing O_2 flow rates to 0.5, 1, and 2 sccm, and the corresponding side length of triangular domains can be as large as ∼10, ∼20, and ∼40 μm (Figure S13). Besides, the surface of as-grown MoS_2 is clean and free of etched triangular pits (Figure 5g−j). MoS_2 domain size increases nearly linearly with growth duration varying from 3, 6, 8, 10, to 14 min (Figure S14).

We have successfully grown uniform monolayer MoS_2 films or large triangular single-crystal domains via OACVD. By introducing O_2 carrier gas, the nucleation density of MoS_2 can be substantially decreased. Triangular single-crystal MoS_2 domains are obtained with side length of ∼350 μm, the largest reported to date. The effect of oxygen during the growth process is systematically demonstrated as an etching reagent, along with preventing poisoning of the MoO_3 precursor powder source. The high RT electron mobility and TEM images of as-transferred MoS_2 demonstrate the ultrahigh quality with relatively low density of defects. Our developed OACVD technique can also be successfully engaged for MoS_2 growth on an amorphous substrate. These high-quality large MoS_2 domains and continuous films provide a promising material platform for applications in electronics and optoelectronics.

■ ASSOCIATED CONTENT

Ⓢ Supporting Information

The Supporting Information is available free of charge on the ACS Publications website at DOI: 10.1021/jacs.5b10519.

Procedures and additional data (PDF)

■ AUTHOR INFORMATION

Corresponding Author

*gyzhang@aphy.iphy.ac.cn

Author Contributions

[‖]W. Chen, J. Zhao, and J. Zhang contributed equally.

Notes

The authors declare no competing financial interest.

■ ACKNOWLEDGMENTS

This work was supported by the 973 Program (Grant Nos. 2013CB934500, 2013CBA01602, 2013CBA01600), the NSFC (Grant Nos. 91223204, 61325021, 91323304, 61390503, 11547139, 51572289, 11574361, 11505032, 11565003), the CAS "Strategic Priority Research Program (B)" (Grant Nos. XDB07010100, XDB07030200), the Natural Science Foundation of Jiangxi Province (Grant Nos. 20151BAB202019, 20142BAB212007), the Science and Technology Project of Jiangxi Provincial Department of Education, and the Bidding Project of Gannan Normal University (Grant Nos. 15zb05, 14zb18).

■ REFERENCES

(1) (a) Baugher, B. W. H.; Churchill, H. O. H.; Yang, Y. F.; Jarillo-Herrero, P. *Nat. Nanotechnol.* **2014**, *9*, 262. (b) Wu, S. F.; Buckley, S.; Schaibley, J. R.; Xu, X. D.; et al. *Nature* **2015**, *520*, 69. (c) Zhang, Y. J.; Oka, T.; Suzuki, R.; Ye, J. T.; Iwasa, Y. *Science* **2014**, *344*, 725. (d) Lee, C. H.; Lee, G.; van der Zande, A. M.; Kim, P.; et al. *Nat. Nanotechnol.* **2014**, *9*, 676.

(2) (a) Radisavljevic, B.; Kis, A.; et al. *Nat. Nanotechnol.* **2011**, *6*, 147. (b) Schmidt, H.; Wang, S.; Chu, L.; et al. *Nano Lett.* **2014**, *14*, 1909.

(3) (a) Zeng, H.; Dai, J.; Yao, W.; Xiao, D.; Cui, X. *Nat. Nanotechnol.* **2012**, *7*, 490. (b) Mak, K. F.; McGill, K. L.; Park, J.; McEuen, P. L. *Science* **2014**, *344*, 1489.

(4) (a) Yin, Z.; Li, H.; Zhang, H.; et al. *ACS Nano* **2012**, *6*, 74. (b) Lopez-Sanchez, O.; Lembke, D.; Kayci, M.; Radenovic, B.; Kis, A. *Nat. Nanotechnol.* **2013**, *8*, 497.

(5) Sangwan, V. K.; Sangwan, V.; Jariwala, D.; Chen, K.; et al. *Nat. Nanotechnol.* **2015**, *10*, 403.

(6) (a) Wu, W. Z.; Lei, W.; Heinz, T.; Wang, Z. L.; et al. *Nature* **2014**, *514*, 470. (b) Zhu, H. Y.; Wang, Y.; Xiao, J.; Zhang, X.; et al. *Nat. Nanotechnol.* **2015**, *10*, 151.

(7) (a) Novoselov, K. S.; Jiang, D.; Schedin, F.; Geim, A.; et al. *Proc. Natl. Acad. Sci. U.S.A.* **2005**, *102*, 10451. (b) Coleman, J. N.; Lotya, M.; Nellist, P.; Nicolosi, V.; et al. *Science* **2011**, *331*, 568.

(8) (a) Najmaei, S.; Liu, Z.; Zhou, W.; Lou, J.; et al. *Nat. Mater.* **2013**, *12*, 754. (b) Van der Zande, A. M.; Huang, P.; Muller, D. A.; Hone, J.; et al. *Nat. Mater.* **2013**, *12*, 554. (c) Zhang, J.; Yu, H.; Chen, W.; Zhang, G.; et al. *ACS Nano* **2014**, *8*, 6024. (d) Yu, Y.; Li, C.; Cao, L. Y.; et al. *Sci. Rep.* **2013**, 3, 1866. (e) Shi, Y. M.; Zhou, W.; Lu, Y.; Kong, J.; et al. *Nano Lett.* **2012**, *12*, 2784. (f) Ji, Q. Q.; Zhang, Y.; Gao, T.; Liu, Z. F.; et al. *Nano Lett.* **2013**, *13*, 3870. (g) Dumcenco, D.; Ovchinnikov, D.; Kis, A.; et al. *ACS Nano* **2015**, *9*, 4611. (h) Liu, K. K.; Zhang, W.; Zhang, H.; Li, L. J.; et al. *Nano Lett.* **2012**, *12*, 1538. (i) Zhan, Y. J.; Zheng, L.; Ajayan, P. M.; Lou, J.; et al. *Small* **2012**, *8*, 966. (j) Balendhran, S.; Ou, J. Z.; Bhaskaran, M.; Sriram, S.; Ippolito, S.; Vasic, Z.; Kats, E.; Bhargava, S.; Zhuiykov, S.; Kalantar-Zadeh, K. *Nanoscale* **2012**, *4*, 461.

(9) Kang, K.; Xie, S.; Huang, P. Y. D.; Park, J.; et al. *Nature* **2015**, *520*, 656.

(10) Huang, C. M.; Wu, S.; Yao, W.; Xu, X. D.; et al. *Nat. Mater.* **2014**, *13*, 1096.

(11) (a) Chhowalla, M.; Amaratunga, G. A. J. *Nature* **2000**, *407*, 164. (b) Remskar, M.; Mrzel, A.; Skraba, Z.; Mihailovic, D.; et al. *Science* **2001**, *292* (5516), 479.

(12) Lee, C.; Yan, H.; Heinz, T.; et al. *ACS Nano* **2010**, *4*, 2695.

(13) Splendiani, A.; Sun, L.; Zhang, Y.; Wang, F.; et al. *Nano Lett.* **2010**, *10*, 1271.

(14) (a) Yamamoto, M.; Einstein, T.; Fuhrer, M. S.; Cullen, W. J. *J. Phys. Chem. C* **2013**, *117*, 25643. (b) Zhou, H. Q.; Yu, F.; Yakobson, B. I.; Tour, J. M.; et al. *Nano Res.* **2013**, *6*, 703.

(15) (a) Lu, J. P.; Carvalho, A.; Castro Neto, A. H.; Sow, C. H.; et al. *Nano Lett.* **2015**, *15*, 3524. (b) Ma, T.; Ren, W.; Ding, F.; Cheng, H. M.; et al. *Proc. Natl. Acad. Sci. U.S.A.* **2013**, *110*, 20386.

(16) Das, S.; Chen, H. Y.; Penumatcha, A. V.; Appenzeller, J. *Nano Lett.* **2013**, *13*, 100.

(17) (a) Radisavljevic, B.; Kis, A. *Nat. Mater.* **2013**, *12*, 815. (b) Liu, H.; Neal, A. T.; Ye, P. D. *ACS Nano* **2012**, *6*, 8563.

(18) (a) Zhou, W.; Zou, X.; Yakobson, B. I.; Idrobo, J. C.; et al. *Nano Lett.* **2013**, *13*, 2615. (b) Zhu, W.; Kong, J.; Xia, F. N.; Avouris, P.; et al. *Nat. Commun.* **2014**, *5*, 3087.